CrystEngComm

Accepted Manuscript

This is an *Accepted Manuscript*, which has been through the Royal Society of Chemistry peer review process and has been accepted for publication.

Accepted Manuscripts are published online shortly after acceptance, before technical editing, formatting and proof reading. Using this free service, authors can make their results available to the community, in citable form, before we publish the edited article. We will replace this *Accepted Manuscript* with the edited and formatted *Advance Article* as soon as it is available.

You can find more information about *Accepted Manuscripts* in the Information for Authors.

Please note that technical editing may introduce minor changes to the text and/or graphics, which may alter content. The journal's standard Terms & Conditions and the Ethical guidelines still apply. In no event shall the Royal Society of Chemistry be held responsible for any errors or omissions in this *Accepted Manuscript* or any consequences arising from the use of any information it contains.

ROYAL SOCIETY OF CHEMISTRY

www.rsc.org/crystengcomm

Cite this: DOI: 10.1039/c0xx00000x

www.rsc.org/xxxxxx

ARTICLE

Controllable growth of novel $BiPO_4$ dendrites by an innovative approach and high energy facets-dependent photocatalytic activity

Qiuying Zhang, Hao Tian, Na Li, Mindong Chen, Fei Teng*

Received (in XXX, XXX) Xth XXXXXXXXX 20XX, Accepted Xth XXXXXXXXX 20XX

DOI: 10.1039/b000000x

For monoclinic $BiPO_4$, it seems fairly difficult to acquire the other novel nanostructures. Herein, we, for the first time, report the controllable syntheses of the six branch- and snowflake-like monoclinic $BiPO_4$ dendrites by ethylenediamine tetraacetic acid. It is surprising that the branch intersection fringes of dendrite have a twinning crystal structure. Moreover, the six branch dendrites show a higher photocatalytic activity than the other two samples, which has been mainly ascribed to its the high-energy (002) facet exposed, high light absorbance, and BET area.The innovative branching growth strategy has made a big breakthrough to fairly fewer nanostructures (only nanoparticles, nanorods and octahedrons available) in the existing references.

1. Introduction

Since properties of materials are strongly dependent on their shapes and sizes, [1,2] a significant progress has been made on the morphology control of materials. [3,4] $BiPO_4$, as an efficient and stable photocatalyst, is most promising to be applied in practice, which has two common crystal phases (monoclinic and hexagonal phases).[5] Furthermore, monoclinic $BiPO_4$ has been demonstrated to have a higher photocatalytic activity than hexagonal one.[5] Up to now, to the best of our knowledge, only the limited nanostructures (octahedrons, nanoparticles and short nanorods) have been synthesized for monoclinic $BiPO_4$.[5-7] It seems fairly difficult to achieve monoclinic $BiPO_4$ with the other new nanostructures. As a result, most of attentions have been paid to ion-doped $BiPO_4$ and $BiPO_4$-based composites, so as to further improve its photocatalytic properties.[8-13] For example, Zhu et al.[9,11] have devoted to the aspect ratio control of $BiPO_4$ nanorods and the preparation of $BiPO_4$-based composites with polyaniline or g-C_3N_4,[12] they have acquired monoclinic $BiPO_4$ short nanorods with the mean length of 300-800 nm and with the aspect ratios of 2-8.[9] Besides, Qian et al. have synthesized the monoclinic $BiPO_4$ nanorods of 0.5-1μm, with the aspect ratios of 4-20. [7] Summarily, only a few of monoclinic $BiPO_4$ nanostructures including octahedrons, nanoparticles and short nanorods can be available in the existing references. It still remains a big challenge to achieve monoclinic $BiPO_4$ with novel nanostructures. It is desirable to explore the novel $BiPO_4$ nanostructure so as to greatly improve their photoactivity. Furthermore, many researches have recently demonstrated that the exposed active facets of catalysts play crucial roles in improving the catalysts activities.[14,15,16] For instance, {110} facets of cubic Ag_3PO_4 are more active than {100} facet;[14] {001} facets of anatase TiO_2 are more active than {101} facets [15] for photocatalytic degradation of rhodamine (RhB); Co_3O_4 nanorods with the {110} facets exposed have the 100% conversion of CO at -70 °C.[17] Generally, the active facets are different for different materials. For $BiPO_4$, the effect of crystal facets on the activity, however, has not been reported up to now. Hence, it is important and desirable to explore and reveal the correlation of active facets with photocatalytic properties of $BiPO_4$. Besides, another significance of this study is that after photoreaction, the branched dendrites are easy to be recycled, since the dendrites can be easily separated from reaction system by filtering or centrifuging. The nanoparticles or short nanorods, nevertheless, are difficult to be recovered by filtering or centrifuging. It is promising to reduce the cost of catalyst used in practice.

Herein, we report the innovative synthesis of the novel snowflake and six-branch $BiPO_4$ dendrites. A plausible branching growth mechanism has been proposed to understand the formation of $BiPO_4$ dendrites. To the best of our knowledge, it is the first report on the synthesis of novel $BiPO_4$ dendrites. Furthermore, the photodegradation of methylene blue (MB) is employed as the probe reaction to investigate their photocatalytic activities[18], and the correlation of the high-energy facets with the photocatalytic activity is mainly revealed.

2. Experiment section

2.1 Chemicals and materials

All chemicals were analytic grade reagents and used without further purification; bismuth nitrate ($Bi(NO_3)_3$), 65% nitric acid (65% HNO_3), disodium edetate-dihydrate (EDTA-Na_2), ethylenediamine tetraacetic acid (EDTA), and sodium phosphate (Na_3PO_4) were purchased from Shanghai Reagents Company (Shanghai, China)

2.2 Preparations

CrystEngComm Accepted Manuscript

$BiPO_4$ cubes: 1mmol $Bi(NO_3)_3$ and 1mmol EDTA-Na_2 was added into 40ml distilled water, and dissolved at 60 °C using water bath heating. Under stirring, the precursor solution became clear, and then 1mmol Na_3PO_4 was added and stirred for 5min again. The resulting precursor suspension was transferred into a Teflon-lined stainless steel autoclave and maintained at 180 °C for 24h. The sample was separated by centrifugation, washed three times with distilled water, and dried at 60 °C for 24h subsequently.

Six-branch $BiPO_4$ dendrites: 1 mmol $Bi(NO_3)_3$ and 1 mmol EDTA was added into 40ml distilled water, and dissolved at 60 °C using water bath heating. Under stirring, the precursor solution became clear, and then 1mmol Na_3PO_4 was added and magnetically stirred for 5min again. The resulting precursor suspension was transferred into a Teflon-lined stainless steel autoclave and maintained at 180 °C for 24h. The sample was separated by centrifugation, washed three times with distilled water, and dried at 60 °C for 24h subsequently.

Snowflake-like $BiPO_4$ dendrites: 1mmol $Bi(NO_3)_3$ and 1 mmol EDTA was added into 40ml nitric acid solution (275 μL of 65wt.% HNO_3 + 40 ml H_2O) at 60 °C using water bath heating. When the precursor solution became clear, 1mmol Na_3PO_4 was added and magnetically stirred for 5min again. The resulting precursor suspension was transferred into a Teflon-lined stainless steel autoclave and maintained at 180 °C for 24 h. The products were washed three times with distilled water and dried at 60 °C for 24 h subsequently.

2.3 Characterization

The prepared precursor and the powders were characterized by a BRUKER D8 X-ray diffraction (XRD) using Cu Ka radiation **(**λ= 0.154nm**)** in a 2θ ranges from 10 ° to 80 ° .The size and morphology were inspected using scanning electron microscopy (SEM, Hitachi SU1510) and a high-resolution transmission electron microscopy (HRTEM). The corresponding selected area electron diffraction (SAED) patterns HRTEM images were obtained on a JEOL-2010 high-resolution TEM performing at 200 kV, and ultraviolet and visible light (UV-Vis) spectra (TU-1901 UV-Vis spectrophotometer).

2.4 Photocatalytic activity measurements

The photocatalytic activities of the samples was evaluated by degradation of MB dye under visible light from a 500 W Xe arc lamp (CEL-HXB F300) equipped with one ultraviolet cutoff filter (λ < 420 nm). The reaction system was placed in a sealed black box with the top opened, and was maintained a distance of 15 cm from the light source. The as-obtained powders (100 mg) were dispersed in 200 mL aqueous solution in a Pyrex beaker containing MB dye (100 mL, 8 mg/L) at room temperature. Before lamp was turned on, the solution was continuously magnetically stirred for 10min in the dark to ensure the establishment of an adsorption–desorption equilibrium between the catalysts and MB solution. During the photocatalytic degradation progress, 3 mL of solution was collected at intervals of irradiation by pipette and subsequently centrifuged to remove the catalysts, and UV-vis adsorption spectra were record on a Shimadzu UV-2500PC spectrometer to determine the concentration of MB.

2.5 Theory calculation

Super cells of $BiPO_4$ crystals are constructed using Material Studios software. All calculations have used the density functional theory (DFT) within the generalized-gradient approximation (GGA), with the exchange-correlation functional of Perdew-Burke-Ernzerh of (PBE). The Castep energy cutoff of 380 eV is adopted. During the relaxations all structures have been relaxed to an energy convergence of 10^{-4} eV (equating to a force convergence of $5x10^{-2}$ eV/Å). In the case of slabs, the vacuum space is larger than 12Å. Surface free energy (γ) is calculated by the following formulae [19,20]:

$$\gamma = (E_{Slab} - N \times E_{BiPO_4}^{Bulk})/2A$$

Where E_{slab} is total energy of the slab, $E_{BiPO_4}^{Bulk}$ is the energy per unit of $BiPO_4$, and N is the total number of unit $BiPO_4$ contained in the super cell.

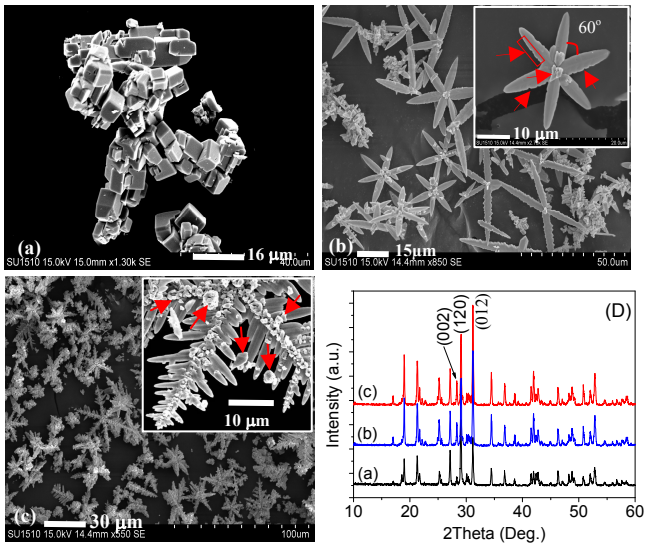

Fig. 1. Scanning electron microscopy (SEM) images and X-ray diffraction (XRD) patterns of the samples prepared at different concentrations of hydrogen ions at 180 °C for 24 h: (a) 0.05 mol L^{-1} EDTA-Na_2, pH=1.3; (b) 0.10 mol L^{-1} EDTA, pH=1.0; (c) 0.10 mol L^{-1} EDTA + 275 μL 65wt.% HNO_3, pH=0.699; (d) XRD. Noting that the insets in (b,c) represent the images at high magnifications; EDTA-Na_2/Bi(III) or EDTA/Bi(III) = 1 (molar ratio)

3. Results and discussion

3.1 Formation of $BiPO_4$ dendrites

In this work, $BiPO_4$ dendrites are synthesized by a facile hydrothermal method without using any templates and surfactants. Herein, ethylene diamine-tetraacetic acid (EDTA) or disodium edetate-dihydrate (EDTA-Na_2) is used as the chelating agent to control the releasing rate of bismuth ions. It is found that the optimal ratio of EDTA/Bi(III) is 1/1 (Figure S1 of electronic supporting information (ESI)). Besides, the temperature-dependent experiment results show that the uniform samples can be only acquired at 180 °C. Therefore, the molar ratio of 1/1 (EDTA/Bi(III)) and 180 °C are used in all the following experiments.

First, we have investigated the microstructures or morphologies of the samples at different concentration of hydrogen ions. At a low concentration of hydrogen ions (0.05 mol L^{-1}, pH=1.3), $BiPO_4$ cubes form, which have the mean sizes

CrystEngComm Accepted Manuscript

This journal is © The Royal Society of Chemistry [year]

of (4~7) × (4~7) × 5 μm (Figure 1a). At a high concentration (0.1 mol L^{-1}, pH=1.0), the unprecedented six-branch dendrites are achieved, whose branches are about 40 × 2 μm (Figure 1b). It is interesting that the intersection angles among the branches are 60 degree (the inset of Figure 1b). Further increasing the concentration of hydrogen ions to 0.20 mol L^{-1} (pH=0.699) by adding HNO_3, the interesting snowflake-like $BiPO_4$ dendrites form, indicating that the further branching growth has occurred (Figure 1c). XRD patterns confirm the formation of phase-pure monoclinic $BiPO_4$ for both samples (Figure 1d). Moreover, the intensity ratios of (012)/(120) peaks are calculated to be 0.74, 1.40 and 1.12 for bulk, six-branch and snowflake dendrites, respectively. The peak intensities of both branched samples are about 1.5-1.9 times as high as that of bulk, indicating (012) facet grows preferentially. At too high concentrations of hydrogen ions (0 and 0.3 mole L^{-1}), phase-pure $BiPO_4$ samples have not formed, but only EDTA are obtained (Figure S2 of ESI). It is clear that the concentration of hydrogen ion has a great influence on the particle morphology. We hold that the concentration of hydrogen ions (*pH*) changes the release rate of Bi(III) ions, because hydrogen ions have shifted the complexing balance of EDTA-Bi(III) complex in aqueous solution (Figure S3 of ESI). Generally, Bi(III) ions can complex completely with EDTA at the stoichiometric ratio and the four hydrogen ions in EDTA molecule are completely released, since $Bi(EDTA)^-$ complex has a high stable constant (K_s=27.94) (Table S1). When the same amount of EDTA-Na_2, instead of EDTA, is used in the experiment, the concentration of hydrogen ions has been measured to be 0.05 mol L^{-1} (*pH*=1.3), in which, $BiPO_4$ cubes are obtained (Figure 1a). When the same amount of EDTA is used, the concentration of hydrogen ions is measured to be 0.10 mol L^{-1} (*pH*=1.0). Under this condition, the six-branch $BiPO_4$ forms (Figure 1b). With further increasing the concentration of hydrogen ions to 0.20 mol L^{-1} (pH=0.699) by adding HNO_3, the snowflake-like $BiPO_4$ dendrites form.

As shown in Figure S4 (ESI), one EDTA molecule has four carboxyl groups (–COOH) and two nitrogen atoms with unshared pair electrons, which not only endows EDTA with the strong chelating ability, but also favors to form hydrogen bond. These structure characteristics facilitate the assembly of complex nanostructures.[19] Due to the formation of bismuth (III)-EDTA complex, bismuth (III) ions can not exist in the form of free ions, which can be firmly confirmed by the fact that the system still maintains clear solution even after sodium phosphate is added. In conventional aqueous solution, the precipitation reaction of the free Bi(III) ions with phosphate ions is too fast to be controlled for the growth of $BiPO_4$. Under hydrothermal conditions, whereas, $Bi(EDTA)^-$ chelates would be broken and the free Bi(III) ions are released slowly, which favors for the controllable growth of $BiPO_4$. The concentration of hydrogen ions, on the other hand, has a great effect on the releasing rate of bismuth (III) ions. Hydrogen ions can combine with both carboxyl groups ($–COO^-$) and nitrogen atoms in EDTA molecule. As a result, Bi(III) ions and hydrogen ions competitively combine with EDTA (Y). Once the free Bi(III) ions are released from $Bi(EDTA)^-$, hydrogen ions would combine with carboxyl groups or nitrogen atoms again. It is well known that EDTA can exist in seven forms at different pH values (Figure S3 of ESI). In our experiment, the pH values of the reaction system are controlled at less than 1.3. According to the distribution diagram of EDTA (Figure S3 of ESI), its main existing form is H_6Y^{2+}, H_5Y^+ and H_4Y at the pH values less than 1.3. A too high concentration of hydrogen ions will reduce the stability of BiY^- chelate. The competitively combining of H^+ and Bi^{3+} with Y processes are described in Equation S1 (ESI).

Hence, at a high concentration of hydrogen ion, most of Bi(III) ions exist in the form of free ions, which favors to produce numerous $BiPO_4$ nuclei and to grow fast. At a low concentration of hydrogen ions, the concentration of free Bi(III) ions is low and more bismuth ions complex with EDTA. Similarly, H_3PO_4 mainly exists as the two forms of H_3PO_4 and $H_2PO_4^-$ at pH values lower than 1.3 (Figure S5 of ESI). Since the Bi(III)-EDTA chelates are soluble in water, the nucleation and growth of $BiPO_4$ are fairly slow, which is strongly dependent on the releasing rate of Bi(III) and $H_2PO_4^-$ ions, instead of mass diffusion. As a result, at a high concentration of hydrogen ions (0.05 mol L^{-1}), the nuclei grow to form the uniform $BiPO_4$ cubes. With moderately increasing the concentration of hydrogen ions, more free bismuth ions are released in the system, which increases growth rate. During the growth process, the bismuth ions near the nuclei are consumed quickly, resulting in a fairly low concentration of Bi(III) ions in the local micro regions. As a result, there is a high concentration difference between the micro regions near the nanocrystals and bulk solution. Hence, the subsequent growth of crystals is strongly dependent on the mass diffusion of bismuth ions from bulk solution to the crystal surfaces. Due to the high surface energy, the apexes, corners and/or ridges of nuclei will grow swiftly, while the others parts of nuclei may grow slowly.[21,22] Thereupon, it is the different growth rates of the different nuclei parts that lead to the formation of the highly-branched dendrites. As for the included angles of 60 degree among branches, we could only conjecture that the six-branch dendrites may grow from the initially formed hexagonal $BiPO_4$ nanocrystals. We have tried to obtain the hexagonal nanocrystal precursors by the time-dependent experiments (Figure S6 of ESI). We can observe that at the initial time the polyhedrons have formed and then they transform into the six-branch crystals through the dissolution and recrystalization processes. The details mechanism is still unknown at the present time. However, our efforts are unsuccessful. It should be noted that no product is acquired at less than 2 h, probably representing that the slow releasing rates of reactive species (Bi(III) and $H_2PO_4^-$ ions). At this time, they have not reached the super saturation for the formation of $BiPO_4$. Up to now, we are still unclear why the included angles among branches are 60 degree. At *pH*=1.0, while the six-branch $BiPO_4$ crystal form, and the secondary nucleation and growth of crystals occur simultaneously. It is reasonable that too more bismuth ions released can form new nuclei, leading the secondary growth. Undergoing the dissolution - recrystallization process, the new secondary branches fully grow. With further increasing the concentration of hydrogen ions by adding HNO_3, more bismuth ions are released. Finally, the highly-branched snowflake-like dendrites form (Figure 1c). Also, some of newly-produced nanocrystals in the system have attached on the surface of every branch, as indicated by the blue arrows (the inset of Figure 1c). The time-dependent experiments of snowflake-like $BiPO_4$ in Figure S7. It is clear that with increasing reaction time,

CrystEngComm Accepted Manuscript

the number of snowflakes increases and the sizes of snowflakes become more uniform, indicating that the dissolution and re-crystallization process have occurred.

Furthermore, Figure 2 shows the high resolution transmission electron microscopy (HRTEM) images of the six-branch and snowflake dendrites. The both sides of individual branch display concavo-convex morphology (Figure 2a). To exactly reveal the fine structure of the branch, we have carefully observed three micro regions, as marked with the red arrows in Figure 2a. In Figure 2b, a lattice spacing of 0.347 nm is determined for the branch head, which corresponds to (020) plane of monoclinic $BiPO_4$. Since the normal of (020) plane is paralleled to the growth direction of the branch, the branch is demonstrated to grow preferentially along the [010] direction. In Figure 2c, the lattice spacings are determined to be 0.238, 0.328 and 0.347 nm, corresponding to (220), (200) and (020) planes of monoclinic $BiPO_4$, respectively. The selected area electron diffraction (SAED) pattern further reveals the single-crystalline nature (the inset of Figure 2c). In Figure 2d, the grain boundary are clear, and two sets of lattice spacings in two intergranular regions have been determined to correspond to (020) plane of monoclinic $BiPO_4$ and (110) plane of hexagonal $BiPO_4$, respectively.[14] Interestingly, SAED pattern (the inset of Figure 2d) confirms the formation of twinning crystal structure at the concavo-convex region (marked by Arrow 3 in Figure 2a). Moreover, the green and red rectangles have been determined to be hexagonal and monoclinic $BiPO_4$, respectively. Zhu et al.[5] have previously reported that under hydrothermal conditions, hexagonal $BiPO_4$ is easy to transform to monoclinic phase at 160 ^oC for 2-3 hours. In our study, however, the hexagonal phase has not transformed into monoclinic one, but exists on the branch. It is a fact that our experimental conditions are different from theirs. In their experiment, the used solvent is glycerin-water mixture; whereas, deionized water and EDTA in our system. It should be noted that, nevertheless, the hexagonal phase has not been detected by XRD in our study (Figure 1d). This may be due to the fairly smaller amount of hexagonal phase than the minimum detecting limit of XRD instrument (≥5%).

At the present time, one key question is how the hexagonal phase affects the branching growth of $BiPO_4$. According to the previous reports on the dendritic crystals,[21,22] a trace of impurities in solution has a significant influence on the crystal growth, which is easily to leads to the formation of dendrites. Hence, we assume that the hexagonal nanocrystals may act as the impurities to induce the branching growth of $BiPO_4$ in our experiment. In order to confirm our conjecture above, the joints between primary and secondary branches of the snowflake-like $BiPO_4$ are observed by HRTEM. The joints between them are clearly observed in Figure 2e, and the lattice fringe image shows that there exists an obvious intergranular boundary between primary and secondary branches (Figure 2f). The interplanar spacing is determined to be 0.349 nm, corresponding to (110) plane of hexagonal $BiPO_4$. This suggests that the hexagonal phase could act as the joint between the primary branch and secondary branch. ED patterns (the inset of Figure 2f) also confirm the twining crystal structure. Compared with Figures 2a and 2e, we could hold that before branching growth, the hexagonal phases have firstly formed on the primary monoclinic branches. With

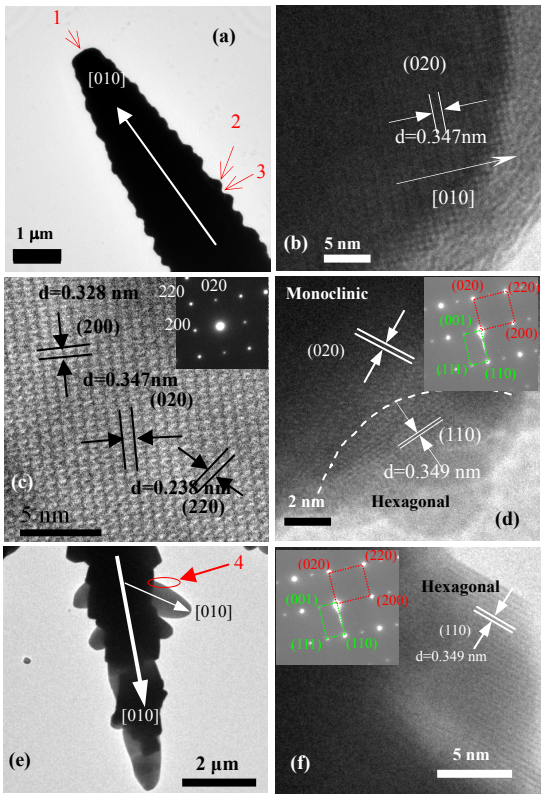

Fig. 2. High-resolution transmission electron microscopy (HRTEM) images of (a-d) six-branch $BiPO_4$ dendrites and (e,f) snowflakes: (a) TEM; (b-d) Lattice fringe images taken from Regions 1-3 marked in Figure 2a (the insets of electron diffraction (ED) patterns in Figure 2c and d)); (f) TEM; (f) Lattice fringe image taken from Region 4 marked in Figure 2e (the inset of ED patterns)

prolonging time, the hexagonal phases grow into the long sub-branches. As a result, the highly branched snowflake-like $BiPO_4$ dendrites form, which consist of both hexagonal sub-branches and monoclinic primary branches. Summarily, the hexagonal nanocrystals not only act as the seeds inducing the secondary branching growth, but also as the joints to connect primary and secondary branches. It should be noted whether the hexagonal phase truly induces the branching growth of $BiPO_4$ or not. The time-dependent experiments have been carried out at pH= 1.0 (Figure S6 of ESI). However, no product can be obtained at less than 2 h. At 2 h, the as-prepared particle seems to be the prototypes of the dendrites, and the branches grow along the directions marked by the red arrows (the inset of Figures S6 of ESI). In Figure S6e, the diffraction peak at about 25^o (2θ) belongs to the (110) plane of hexagonal $BiPO_4$ (JCPDS: 45-1370), indicating that the monoclinic and hexagonal phases coexist in the sample. So we assume that hexagonal phase, as the growing seeds, may exist in the initial stages (the insets of Figure 5Sa,b). With prolonging the reaction time, the hexagonal phase transforms to monoclinic phase (Figure S6). If the concentration of hydrogen ions is high enough, the releasing rate of bismuth ions is so fast that hexagonal $BiPO_4$ cannot completely change into monoclinic phase in time. Thus, the hexagonal phase, as the seed, induces the further branching growth.

CrystEngComm Accepted Manuscript

This journal is © The Royal Society of Chemistry [year]

3.2 Facet-dependent photocatalytic activity

Observed from Figure 3, the six-branch dendrites have a higher photocatalytic activity (72.8%) than the snowflake dendrites (45.9%) and cubes (35.1%) after 40-min irradiation (λ< 420 nm). The apparent rate constants (k_a) of six-branch dendrites, snowflake dendrites and cubes are 0.02941, 0.01532 and 0.01321 min^{-1}, respectively. The apparent rate constant of the six-branch dendrites is 0.92 and 1.23 times higher than those of the latter two, respectively. Three important factors are mainly considered. First, UV-visible light diffuse reflection spectra (UV-DRS) (Figure S8) show that the six-branch dendrites have a higher absorbance capability than the snowflakes, which favors to fully utilize ultraviolet light that favor for the irradiation of charge carriers. Second, the BET areas of cubes and six-branch dendrites are 7.9 and 6.5 $m^2 g^{-1}$, respectively; which are higher than that (3.2 $m^2 g^{-1}$) of the snowflakes (Table S2 of ESI).

Furthermore, we have calculated the surface energies of the typical (002), (020) and (200) facets using Materials Studio Software (Figure 4). The surface energies of (002), (020) and (200) facets are 1.41, 0.68 and 0.66 J/M^2 (Figure S9 of ESI). It has been demonstrated that the high-energy (002) facets are expected to more active than the others. [3,14,17] We have determined that the numbers of Bi(III) ions, as well suspending oxygen, are 27, 18 and 18 on (002), (020) and (200) facets, respectively. The Bi(III) ions on the exposed facets are generally unsaturated, which favor for the adsorption of dyes[23]. Moreover, more suspended oxygen atoms on the exposed (002) facets could catch the irradiated electrons, which favors for the separation of charge carriers. As a result, the high-percentage (002) facets benefit to the improvement of activity for the six-branch dendrites.

Besides, the branches surfaces are clean for the six-branch dendrites; whereas, on the branches surfaces are the nanoparticles attached for the snowflakes. The nanoparticles have been demonstrated to be hexagonal $BiPO_4$ by HRTEM. Zhu et al. have demonstrated that hexagonal $BiPO_4$ have a lower activity than monoclinic one. [5] All the factors above contribute to the improved activity of the six-branch $BiPO_4$ dendrites.

Furthermore, the nanoparticles are usually separated from the photoreaction system at low recovery efficiency by filtering or centrifuging, leading to a significant mass loss is. Our highly-branched dendrites, nevertheless, are easy to be separated from reaction system simply by filtering or centrifuging, in which the recycle efficiency of photocatalyst can reach 99.5 wt% after photoreaction. This is greatly important to reduce the cost of catalyst applied in practice.

4. Conclusions

To conclude, we have developed an innovative method to acquire the novel monoclinic $BiPO_4$ dendrites, in which the initially formed hexagonal phase induces the secondary branching growth. Future research will be carried out to reduce the sizes of monoclinic $BiPO_4$ dendrites to further improve the photocatalytic activity.[24]

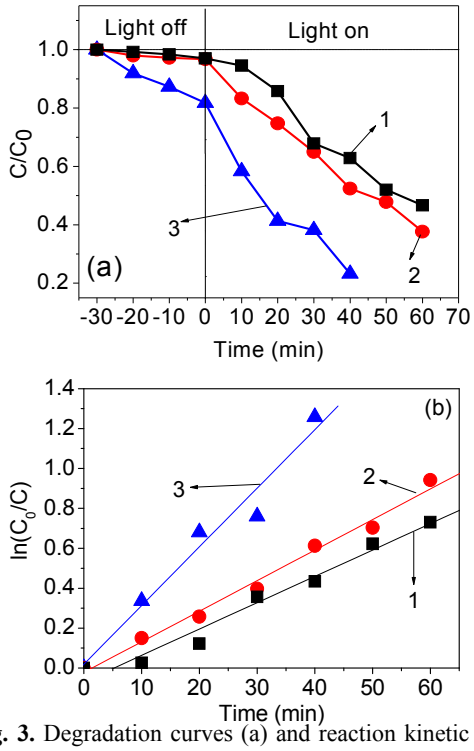

Fig. 3. Degradation curves (a) and reaction kinetic curves (b) of the samples for methylene blue (MB) under UV-light irradiation (λ < 420 nm): 1, Cubes; 2, Snowflakes; 3, Six-branch dendrites

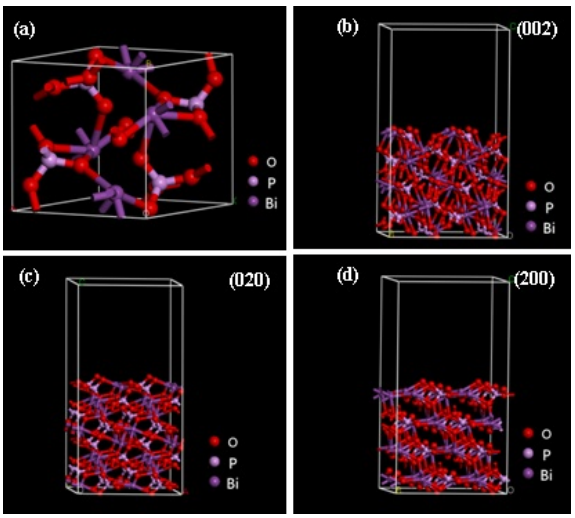

Fig. 4 Calculation modes of monoclinic $BiPO_4$ by Material Studios software: (a) Super cell units; (b-d) Atomic configuration of (020), (200) and (002) facets

Acknowledgements

This work is financially supported by National Science Foundation of China (21377060, 21103049), Six Talent Climax Foundation of Jiangsu (20100292), Jiangsu Science Foundation of China (BK2012862), Jiangsu Province of Academic Scientific Research Industrialization Projects (JHB2012-10, JH10-17), the Key Project of Environmental Protection Program of Jiangsu (2013016, 2012028), the Project Funded by the Science and Technology Infrastructure Program of Jiangsu (BM2013139, 201380277), the Project of Foreign Culture and Education expert

CrystEngComm Accepted Manuscript

(N0502001003), Teaching Reform Project to Enhance the Practice Innovation of NUIST-2013 (N1885013014), Support Program for Undergraduate Dissertation of NUIST-2013 (N1085002008), A Project Funded by the Priority Academic Program Development of Jiangsu Higher Education Institutions (PAPD), and Jiangsu Province Innovation Platform for Superiority Subject of Environmental Science and Engineering sponsored by SRF for ROCS, SEM (2013S002), and "333" Outstanding Youth Scientist Foundation of Jiangsu (2011015).

Notes and references

Jiangsu Engineering Technology Research Centre of Environmental Cleaning Materials, Jiangsu Key Laboratory of Room Environment Monitoring and Pollution Control, Innovative research Laboratory of Environment and Energy, School of Environmental Sciences and Engineering, Nanjing University of Information Sciences and Engineering, Nanjing 210044, China. Corresponding author. Email: tfwd@163.com (F. Teng); Phone: 86-25-58731090

† Electronic Supplementary Information (ESI) available: Distribute diagrams of EDTA and H_3PO_4, UV-vis, SEM images of the products obtained at different reaction periods, BET, XRD patterns, calculation results using Materials Studio software, etc. This material is available free of charge via the internet at http://pub.rsc.com

1. T. R. Gordon, M. Cargnello, T. Paik, F. Mangolini, R. T. Weber, P. Fornasiero and C. B Murray, J. Am. Chem. Soc., 2012, **134**. 6751.
2. M.Xu, J. T. Zai, Y. P. Yuan, X. F. Qian, J. Mater. Chem., 2012, **22**, 23929
3. H. G. Yang, C. H. Sun, S. Z. Qiao, J. Zou, G. Liu, S. C. Smith, H. M. Cheng and G. Q. Lu, Nature, 2008, **453**, 638.
4. T. Nonoyama, T. Kinoshita and M. Higuchi, J. Am. Chem. Soc., 2012, **134**, 8841.
5. Y. F. Liu, X.G Ma, X Yi and Y. F. Zhu, Acta Phys.-Chim. Sin., 2012, **283**, 654.
6. C. S. Pan and Y. F. Zhu, J. Mater. Chem., 2011, **21**, 4235.
7. F. Xue, H. B. Li, Y. C. Zhu, S. L. Xiong, X. W. Zhang, T. T. Wang, X. Liang and Y. T. Qian, J. Solid State Chem., 2009, **182**(6), 1396.
8. T. Lv, L. K. Pan, X. J. Liu and Z. Sun, RSC Adv., 2012, **2**, 12706.
9. J. Geng, W. H. Hou, Y. N. Lv, J. J. Zhu and H. Y. Chen, Inorg. Chem., 2005, **44**, 8503.
10. M. L. Zhao, G. S. Li, J. Zheng, L. P. Li, H. Wang and L. S. Yang, CrystEngComm., 2011, **13**, 6251.
11. Y. N. Zhang, H. Q. Fan, M. M. Li and H. L. Tian, Dalton Trans., 2013, **42**, 13172.
12. C. S. Pan, J. Xu, Y. J. Wang, D. Li and Y. F. Zhu, Adv. Funct. Mater., 2012, **22**, 1518.
13. H. Xu, Y. G. Xu, H. M. Li, J. X. Xia, J. Xiong, S. Yin, C. J. Huang and H. L. Wan, Dalton Trans., 2012, **41**, 3387.
14. S. Boddu, B.-V. Naidu, S. Vasanthakumaran and K. V. Rajesh, Dalton Trans., 2012, **41**, 3194.
15. J. Wang, F. Teng, M. D. Chen, J. J. Xu, Y. Q. Song and X. L. Zhou, CrystEngComm., 2013, **15**, 39.
16. J. Shen, J. T. Zai, Y. P. Yuan, X. F. Qian, Int J Hydrogen Energ, 2012, **37**, 16986
17. Q. J. Xiang and J. G. Yu, Chin., J. Catal. 2011, **32**, 525.
18. S. S. Ma, J. J. Xue, Y. M. Zhou, Z. W. Zhang, J. Mater. Chem. A, 2014, **2**,7272
19. X. W. Xie, Y. Li, Z. Q. Liu, H. Masatake and W. J. Shen, Nature 2007, **458**, 746.
20. B. Romero, S. Bruque, M. A. G. Aranda and J. E. Iglesias, Inorg. Chem., 1994, **33**, 1869.
21. L. Xu, X. Y. Yang, Z. Zhai and W. H. Hou, CrystEngComm., 2011, **13**, 7267.
22. J. Nelson, Cryst. Growth Des., 2005, **5**(4), 1509.
23. T. Y. Zhao, J. T. Zai, M. Xu, Q. Zou, Y. Z. Su, K. X. Wang, X. F. Qian, CrystEngComm., 2011, **13**, 4010
24. J. T. Zai, J. Zhu, R. R. Qi, X. F. Qian, J. Mater. Chem. A, 2013, **1**, 735

CrystEngComm Accepted Manuscript

This journal is © The Royal Society of Chemistry [year]